ISSN: 2689-1204

Research Article

Journal of Applied Material Science & Engineering Research

Numerical Analysis of ZnO Thin Film Crystallographic Stability on Metal Substrates

Salah Uddin[1]* and Md. Miraj Hossain[2]

[1]*Department of Electrical and Electronic Engineering, Feni University, Bangladesh*

[2]*Tokyo University of Foreign Studies, Japan*

***Corresponding Author**
Salah Uddin, Department of Electrical and Electronic Engineering, Feni University, Bangladesh.

Submitted: 2026, Aug 26; **Accepted:** 2026, Sep 17; **Published:** 2026, Sep 23

Citation: Uddin, S., Hossain, M. M. (2026). Numerical Analysis of ZnO Thin Film Crystallographic Stability on Metal Substrates. *J App Mat Sci & Engg Res, 10*(1), 1- 07.

Abstract

We present a density functional theory (DFT) investigation of the crystallographic stability and formation energetics of ultrathin ZnO films on Ag(111), Ag(001), and Pt(001) metal substrates. DFT calculations using the Vienna Ab Initio Simulation Package (VASP) with the Perdew−Burke−Ernzerhof (PBE) exchange-correlation functional and Grimme D2 dispersion correction predict that the ZnO film structure is governed jointly by the substrate surface symmetry and the film/substrate lattice mismatch. The relative formation energy per unit area systematically favors wurtzite (O-terminated, E_{pox}%/A = −83.6 meV/Å²) on Ag(111) and zinc-blende (O-terminated, E_{pox}%/A = −160.4 meV/Å²) on Pt(001). These findings are in quantitative agreement with experimental observations from HRTEM and LEED, establishing clear design rules for engineering ZnO phase selection via substrate choice.

Keywords: ZnO Thin Films, DFT, VASP, Wurtzite, Zinc-Blende, Formation Energy, Lattice Mismatch, Ag(111), Pt(001), Surface Symmetry

1. Introduction

A significant amount of research has been done on ZnO nanostructures because they could be useful as a material in many areas, such as solar cells, light-emitting diodes, photocatalysis, gas sensors, catalysis, laser diodes, varistors, and sensors [1-9]. It is well known that ZnO is an n-type semiconductor with a significant band gap of about 3.37 eV and a large exciton binding energy of about 60 meV at room temperature [10-15]. There are, however, some problems with using these methods for ZnO nanoparticles. These include high temperatures, precise gas concentrations, dangerous chemicals, and expensive tools [16-24].

Thin oxide films grown on metal supports are a model system for exploring structural and electronic properties at the nanoscale [25-36]. ZnO thin films in particular have attracted significant interest due to their versatile properties a wide band gap (3.37 eV), high exciton binding energy (60 meV), piezoelectric behavior, and catalytic activity which make them promising for sensors, transducers, optoelectronic devices, and heterogeneous catalysis.

The structural polymorphism of ZnO is well documented. Under ambient conditions, ZnO adopts the wurtzite structure with a hexagonal lattice (a = 3.25 Å, c = 5.21 Å) and ionic character arising from Zn in tetrahedral coordination. A zinc-blende phase has been stabilized in thin films on cubic substrates, while the rock-salt phase appears under pressures above ~10 GPa For ultrathin films on metal supports, an additional graphitic-like (flat, sp²-bonded) phase can emerge [37-50].

The influence of the metal substrate on the ZnO film structure has been studied extensively for Pt(111), Ag(111), Au(111), and Cu(111) surfaces.[2Ḥ10Ḥ11] Recent DFT+U calculations for ZnO on Cu(111) revealed a transition from graphitic to wurtzite-like structure beginning at 5 layers, driven by charge transfer from the metal to the oxide. However, the comparative role of substrate symmetry (hexagonal vs square) versus lattice mismatch in determining ZnO film structure remains incompletely understood. In this work, we present systematic DFT calculations of ZnO relative formation energies on Ag (111), Ag (001), and Pt (001) substrates, spanning both wurtzite and zinc-blende structural candidates. Our results, validated against companion HRTEM and LEED measurements, provide a predictive framework for phase

engineering of ZnO ultrathin films.

2. Computational Methods

Density functional theory (DFT) calculations were performed using the Vienna Ab Initio Simulation Package (VASP).[16]Ң[17] The projector-augmented wave (PAW)[18]Ң[19] method was used to describe the interactions between nuclei and core electrons. The valence electrons treated explicitly were: Zn (3d, 4s), O (2s, 2p), Ag (4d, 5s), and Pt (5d, 6s). The Perdew-Burke-Ernzerhof (PBE) approximation was employed for the exchange-correlation functional. Dispersion forces were included via Grimme's D2 method.

The reciprocal space sampling was performed on a 2 × 2 × 1 Γ-centered k-point mesh. A 400 eV plane-wave cutoff energy was used, chosen to ensure well-converged calculations with negligible Pulay forces. Selected convergence tests using a 600 eV cutoff showed variations of only ~3 meV/Å² in relative formation energies, confirming the adequacy of the 400 eV value. Electronic energy convergence was achieved to within 10^{-6} eV, and ionic relaxation was stopped when all forces were below 0.01 eV/Å under the conjugate-gradient algorithm.

2.1. Slab Models

Fully relaxed DFT calculations were performed on coincidence ZnO/metal slabs. These slabs correspond to combinations of m × m metal surface unit cells and (m−1) × (m−1) freestanding ZnO unit cells, chosen to minimize the artificial strain at the interface. Four ZnO layers were used to model the thin film, while the metal substrate was represented by two layers fixed in bulk positions [25,33].

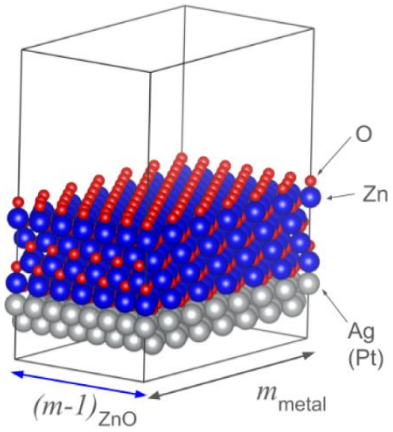

Figure 1: Coincidence ZnO/metal slabs: a 4-layer slab composed of (m−1) × (m−1) cells of ZnO over a 2-layer slab composed of m × m cells of metal (Ag or Pt).

Preliminary calculations confirmed that a 4-metal-layer model with the two topmost layers free to relax produced negligible displacements of the Ag atoms (compatible with the 2-layer fixed model). The illustration of the model used is reported in Figure 1. The computed work function of the Ag slab using this model is 4.352 eV, in good agreement with the experimental value of 4.46 eV.

For the wurtzite/Ag(111) calculation, we set m = 7, giving: 7 × 2.89 Å = 20.23 Å for the Ag(111) layer and 6 × 3.4 Å = 20.4 Å

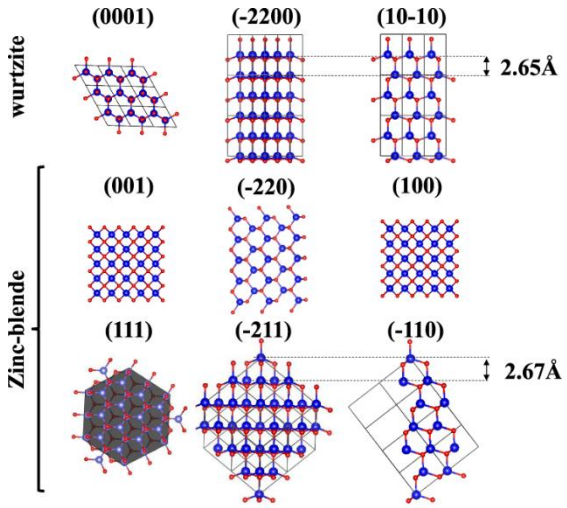

Figure 2: Atomic distribution and distances within the wurtzite planes: (0001), (−2200), and (10−1 0); and zinc-blende planes: (001), (−220), (100), (111), (−211), and (−110). Key interatomic distances are highlighted. CIF files from ref.

for the ZnO layer, where 3.4 Å and 2.89 Å are the experimental lattice parameters for wurtzite ZnO and Ag(111), respectively. Experimental in-plane lattice parameters were used as constraints throughout. The lateral reconstruction at the interface was introduced by hand to reduce the computational unit cell size and avoid Moiré supercells.

In the ZnO film grown on reconstructed Pt(001), the hexagonal surface reconstruction of Pt was not considered in the calculations, as the post-annealing procedure used to ensure crystallinity of the film likely lifts this reconstruction, a behavior already demonstrated for iron oxide thin films on the same surface [24,30].

2.2. Formation Energy

Relative formation energies per unit area were calculated according to:

$$E_{form} = E_{TOT} - m^2 E_M - (m-1)^2 E_{ZnO} \quad (1)$$

where E_{tot} is the total energy of the coincidence ZnO/metal slab, E_m is the energy of the 1 × 1 metal surface, E_{4n0} is the energy of the freestanding 1 × 1 ZnO slab, and A is the surface area. This formulation isolates the interaction contribution of the ZnO film with the metal substrate, normalized per unit interface area.

3. Results and Discussion

3.1. Crystallographic Phase Analysis

Figure 2 shows the atomic distribution within (0001), (−2200), and (10−1 0) planes for wurtzite and (001), (−220), (100), (111), (−211), and (−110) planes for zinc blende. The comparison of (0001) and (001) planes clearly evidence different atomic symmetry (hexagonal vs square) and interatomic distances between the two phases. Importantly, the wurtzite (0001) and zinc-blende (111) sections share nearly identical symmetry and interatomic distances (differing by only 0.01 Å), while (10−1 0) for wurtzite and (−110) for zinc blende show clearly different periodicities along the vertical axis: 5.31 Å and 8.02 Å, respectively. This degeneracy in the surface-accessible planes demonstrates why LEED alone cannot distinguish between wurtzite and zinc-blende phases in ZnO thin films, motivating the use of DFT formation energy calculations in conjunction with cross-sectional TEM.

3.2. Formation Energies: Wurtzite vs Zinc Blende

Table 1 summarizes the relative formation energies per unit area for all calculated ZnO/metal slab configurations. Several clear trends emerge from these results:

On Ag (111), the O-terminated wurtzite structure is the most stable (E_{form} ox a⁄c/A = −83.6 meV/Å²), followed by O-terminated zinc blende (−74.7 meV/Å²) and Zn-terminated wurtzite (−30.0 meV/Å²). The energy difference between O-terminated wurtzite and zinc blende is approximately 9 meV/Å², well above the numerical uncertainty of ~3 meV/Å². Over a representative 5.5 nm × 5.5 nm area such as that imaged in the HRTEM experiments, this energy difference amounts to approximately 30 eV — a thermodynamically significant value.

On Pt (001), the O-terminated zinc-blende structure is strongly preferred (E_{form} ox a⁄c/A = −160.4 meV/Å²), more than three times more negative than the O-terminated wurtzite (−45.0 meV/Å²). This dramatic stabilization of zinc blende on the square-symmetric Pt (001) surface establishes that substrate geometry, not just composition, is the primary determinant of ZnO film structure. On Ag(001), the zinc-blende phase is also preferred (−107.5 meV/Å² vs −67.0 meV/Å² for Zn-terminated wurtzite), reinforcing that square-symmetric substrates drive zinc-blende formation regardless of the specific metal.

ZnO/metal	Termination	Eform/A [meV/Å²]
graphitic/Ag(111)	O	−31.5
wurtzite/Ag(111)	O	−83.6
wurtzite/Ag(111)	Zn	−30.0
wurtzite/Ag(001)	Zn	−67.0
wurtzite/Pt(001)	O	−45.0
zinc blende/Ag(111)	O	−74.7
zinc blende/Pt(001)	O	−160.4
zinc blende/Ag(001)	O	−107.5

Table 1: Termination and Relative Formation Energy per Area Unit for ZnO/Metal Slabs (m = 7)

3.3. Structural Details of the Predicted Phases

For ZnO wurtzite on Ag (111), the calculated O-terminated structure shows an interatomic distance of 2.65 Å along the (111) direction, while the Zn-terminated structure gives 2.55 Å. The O-terminated termination is identified as the most probable, consistent with both the lower formation energy and the atomic distribution observed in STEM images from the companion experimental study.

For ZnO zinc blende on Pt (001), the zinc-blende structure requires only a small in-plane lattice parameter stretch and modification of out-of-plane lattice parameters of up to 2%, accommodating the mismatch between the ZnO(111) plane (3.3 Å in-plane lattice parameter) and the Pt(001) surface (2.8 Å lattice parameter). The relative formation energy of zinc blende on Pt(001) (−160.4 ± 3.0 meV/Å²) is substantially more negative than wurtzite (−45.0 ± 3.0 meV/Å²), providing a clear theoretical prediction confirmed experimentally.

3.4. Role of Substrate Symmetry and Lattice Mismatch

Our systematic calculations allow us to decouple the effects of substrate symmetry and lattice mismatch on ZnO phase stability. The data in Table 1 demonstrate that: (i) hexagonal substrates (Ag (111)) favor wurtzite; (ii) square substrates (Ag (001), Pt (001)) favor zinc blende. This trend holds across substrates of different compositions (Ag vs Pt), indicating that surface symmetry is the dominant factor.

The lattice mismatch modulates the magnitude of the formation energy: the larger mismatch on Pt(001) correlates with the more negative zinc-blende formation energy (−160.4 meV/Å² vs −107.5 meV/Å² on Ag(001)), suggesting that epitaxial strain energy can be released more effectively in the zinc-blende phase on Pt(001). The formation energies calculated for ZnO on Ag(111) are of comparable magnitude to previous DFT results: ~50 meV/Å² for ZnO wurtzite on Cu(111)[1] and 37−55 meV/Å² for ZnO bilayers on Cu(111), Ag(111), and Au(111).[28]

Regarding in-plane atomic registry, our calculations show that the film/substrate lattice mismatch prevents a unique identification of preferential Zn atom sites (on-site, hollow, or interstitial) over the metal substrate unit cell. The in-plane section of the ZnO film over the silver substrate reveals a gradual change in relative position of Zn atoms with respect to substrate atoms across the coincidence unit cell — consistent with the absence of Moiré patterns in the LEED data and supporting the experimental in-plane lattice parameter constraints used in the model.

Our finding that zinc-blende ZnO can be stabilized solely by substrate symmetry extends the known range of systems in which this metastable phase occurs. Previously, zinc-blende ZnO had been observed only on GaAs substrates with ZnS buffer layers [1,2]. The capability to engineer the ZnO surface structure through substrate design is valuable for catalytic and optoelectronic applications.

4. Conclusions

DFT calculations using VASP with PBE exchange-correlation and Grimme D2 dispersion correction establish that the crystallographic phase of ZnO ultrathin films is determined by a combination of substrate surface symmetry and lattice mismatch. Hexagonal (111) substrates favor wurtzite (O-terminated, Eform/A = −83.6 meV/Å² on Ag(111)), while square-symmetric substrates favor zinc-blende (Eform/A = −160.4 meV/Å² on Pt(001)). The energy differences are thermodynamically significant (≥30 eV over nm-scale areas) and unambiguous relative to the numerical uncertainty of ~3 meV/Å². These predictions are fully consistent with HRTEM and LEED data from the companion experimental study and provide predictive design rules for engineering ZnO thin-film phase selection through substrate choice.

References

1. Abbas, F. I., Tsuchiyama, T., & Sugiyama, M. (2026). Correlation of zinc oxide (ZnO) thin film fabrication and interface functionality by novel electrostatic spray deposition. *International Journal of Nanoscience,* 2640020.
2. Abbas, F. I., & Sugiyama, M. (2026). Comprehensive investigation on nickel oxide (NiO) thin film fabrication mechanism by electrostatic spray deposition (ESD) technique and annealing temperature effect on NiO/ZnO diodes. *Physica B: Condensed Matter,* 418507.
3. Abbas, F. I., & Sugiyama, M. (2025). Investigation of the Solution-Dependent Zinc Oxide (ZnO) Thin Film Growth Process by the Electrostatic Spray Deposition (ESD) Method. *Journal of Materials Science and Chemical Engineering*,

13(9), 96-114.
4. Abbas, F. I., & Sugiyama, M. (2025). ZnO-Thin Film Growth Processes: Correlation Between the Structural Properties of Hydrochloric Acid (HCl) and Water (H2O) Solution Effect Using Innovative Electrostatic Spray Deposition (ESd) Technology. *Latvian Journal of Physics and Technical Sciences, 62*(3), 68-76.
5. Abbas, F. I., & Sugiyama, M. (2024). A Comparative Study of Property Measurement for ZnO-Thin Film Growth Processes Using Hydrocloric Acid (HCl) and Water (H2O) Solution-Dependent on Novel Electrostatic Spray Deposition (ESD). *Latvian Journal of Physics and Technical Sciences, 62*(2), 30-41.
6. Abbas, F. I., & Sugiyama, M. Comprehensive Investigation on Nickel Oxide (Nio) Thin Film Growth Mechanism by Electrostatic Spray Deposition (Esd) Technique and Annealing Temperature Effect on Nio: Hcl/Zno: Hcl Diodes. Zno: Hcl Diodes.
7. Abbas, F. I., & Sugiyama, M. (2025). Anisotropic role on zinc oxide (ZnO) thin film growth processes of solution-dependent novel electrostatic spray deposition (ESD). *European Journal of Engineering and Technology Research, 10*(2), 1-8.
8. Abbas, F. I., Sugiyama, M. (2025). Investigation the Anisotropic Feature Using Structural and Mechanical Profile Analysis of Zinc Oxide (ZnO) Thin Film Growth Mechanism within the Framework of Williamson-Hall Estimation by Novel Electrostatic Spray Deposition (ESD) Technique. J. Phy.: App. *Mechanics, 1*, 1-9.
9. Abbas, F. I., & Sugiyama, M. (2024). Solution-dependent electrostatic spray deposition (ESD) ZnO thin film growth processes. arXiv preprint arXiv:2406.13313.
10. Thang, H. V., Tosoni, S., & Pacchioni, G. (2019). The epitaxial growth of ZnO films on Cu (111) surface: Thickness dependence. *Applied Surface Science, 483*, 133-139.
11. Bieniek, B., Hofmann, O. T., & Rinke, P. (2015). Influence of hydrogen on the structure and stability of ultra-thin ZnO on metal substrates. *Applied Physics Letters, 106*(13).
12. Ta, H. Q., Zhao, L., Pohl, D., Pang, J., Trzebicka, B., Rellinghaus, B., ... & Rümmeli, M. H. (2016). Graphene-like ZnO: A mini review. *Crystals, 6*(8), 100.
13. Wang, Z. L. (2004). Zinc oxide nanostructures: growth, properties and applications. *Journal of physics: condensed matter, 16*(25), R829-R858.
14. Kresse, G., & Furthmüller, J. (1996). Efficiency of ab-initio total energy calculations for metals and semiconductors using a plane-wave basis set. *Computational materials science, 6*(1), 15-50.
15. Kresse, G., & Furthmüller, J. (1996). Efficient iterative schemes for ab initio total-energy calculations using a plane-wave basis set. *Physical review B, 54*(16), 11169.
16. Blöchl, P. E. (1994). Projector augmented-wave method. *Physical review B, 50*(24), 17953.
17. Kresse, G., & Joubert, D. (1999). From ultrasoft pseudopotentials to the projector augmented-wave method. *Physical review b, 59*(3), 1758.
18. Perdew, J. P., Burke, K., & Ernzerhof, M. (1996). Generalized gradient approximation made simple. *Physical review letters, 77*(18), 3865.
19. Grimme, S. (2006). Semiempirical GGA-type density functional constructed with a long-range dispersion correction. *Journal of computational chemistry, 27*(15), 1787-1799.
20. Chelvayohan, M., & Mee, C. H. B. (1982). Work function measurements on (110),(100) and (111) surfaces of silver. *Journal of Physics C: Solid State Physics, 15*(10), 2305-2312.
21. Ascrizzi, E., Goniakowski, J., Yang, J., Agnoli, S., & Ferrari, A. M. (2024). DFT study of the moiré pattern of FeO monolayer on Au (111). *Physical Chemistry Chemical Physics, 26*(29), 20103-20111.
22. Davis, E. M., Zhang, K., Cui, Y., Kuhlenbeck, H., Shaikhutdinov, S., & Freund, H. J. (2015). Growth of Fe3O4 (001) thin films on Pt (100): Tuning surface termination with an Fe buffer layer. *Surface Science, 636,* 42-46.
23. Liu, B. H., Boscoboinik, J. A., Cui, Y., Shaikhutdinov, S., & Freund, H. J. (2015). Stabilization of ultrathin zinc oxide films on metals: Reconstruction versus hydroxylation. *The Journal of Physical Chemistry C, 119*(14), 7842-7847.
24. Richard, A., & Corà, F. (2023). Influence of dispersion interactions on the polymorphic stability of crystalline oxides. *The Journal of Physical Chemistry. C, Nanomaterials and Interfaces, 127*(22), 10766.
25. Abbas, F. I., Chakraborty, S., & Sugiyama, M. (2026). First principle applications to investigate the thermodynamic of mixing and transport phenomena for Al 1− x Au x binary liquid alloy. *International Journal of Modern Physics B, 40*(13), 2650111.
26. Abbas, F. I., Chakraborty, S., Sugiyama, M., Samad, M., Khan, A. R. (2025). A Microscopic Investigation on Atomic Transport Properties for Liquid Al. *J App Mat Sci & Engg Res, 9*(2), 01-05.
27. Abbas, F. I., Chakraborty, S., & Sugiyama, M. (2026). First principle applications to investigate the thermodynamic of mixing and transport phenomena for Al 1− x Au x binary liquid alloy. *International Journal of Modern Physics B, 40*(13), 2650111.
28. Abbas, F. I., & Bhuiyan, G. M. (2023). Atomic transport properties and liquid–liquid phase separation of Zn x Bi 1− x liquid monotectic alloys. *Journal of Physics: Condensed Matter, 35*(32), 324001.
29. Abbas, F. I., & Bhuiyan, G. M. (2022). A study of thermodynamics of mixing for Al1− xZnx liquid binary alloy. *Physica B: Condensed Matter, 647,* 414365.
30. Abbas, F. I., Bhuiyan, G. M., & Kasem, R. (2020). Critical Properties of Segregation for Al1− x Bi x Liquid Binary Alloys. *Journal of the Physical Society of Japan, 89*(11), 114004.
31. Bhuiyan, G. M., & Abbas, F. I. (2019). Local minimum in pair potentials of polyvalent metals: A limitation of pseudopotential theory. *International Journal of Modern Physics B, 33*(07), 1950049.
32. Abbas, F. I., & Bhuiyan, G. M. (2023). Atomic transport properties and liquid–liquid phase separation of Zn x Bi 1− x liquid monotectic alloys. *Journal of Physics: Condensed*

Matter, 35(32), 324001.
33. Abbas, M. F. I. (2019). Thermodynamic and transport properties of aluminium (Al)-based liquid binary alloys (Doctoral dissertation, University of Dhaka).
34. Abbas, F. I., Bhuiyan, G. M., & Kasem, M. R. (2018). A study of thermodynamics of mixing for Al1− xSnx liquid binary alloy. *Journal of non-crystalline solids, 481*, 391-396.
35. Bhuiyan, G. M., & Abbas, F. I. (2017). Local minimum in effective pairpotentials: Pseudopotential theory revisited. *arXiv preprint arXiv:*1710.07931.
36. Abbas, F. I., Bhuiyan, G. M., & Ahmed, A. Z. (2016). Energy of mixing and entropy of mixing for Cu $ _ {x} $ Al $ _ {1-x} $ liquid binary alloys. *arXiv preprint arXiv*:1607.05827.
37. Al Rakib, M. A., Samad, M. F., Rahman, M. M., Abbas, F. I., Samad, M., Rahman, M. A., ... & Abbas, F. I. (2023). Cost effective weather monitoring station. *European Journal of Engineering and Technology Research, 8*(2), 73-78.
38. Al Rakib, M. A., Rahman, M. M., Hossain, M. M., Rahman, M. A., Samad, M., & Abbas, F. I. (2022). Induction motor based speed and direction controller. *European Journal of Engineering and Technology Research, 7*(6), 82-86.
39. Al Rakib, M. A., Rahman, M. M., Uddin, S., Khan, M. A. H., Rahman, M. A., Hossain, M. M., ... & Abbas, F. I. (2022). Smart agriculture robot controlling using bluetooth. European Journal of Engineering and Technology Research, 7(6), 77-81.
40. Al Rakib, M. A., Rahman, M. M., Rahman, M. A., Chakraborty, S., Shawon, M. A. S., & Abbas, F. I. (2021). IoT based controlling of power grid. *European Journal of Engineering and Technology Research, 6*(6), 54-57.
41. Al Rakib, M. A., Rahman, M. M., Uddin, S., Anik, M. S. A., Talukder, A. H., Samad, M., & Abbas, F. I. (2022). Fingerprint based smart home automation and security system. *European Journal of Engineering and Technology Research, 7*(2), 140-145.
42. Al Rakib, M. A., Rahman, M. M., Anik, M. S. A., Masud, F. A. J., Islam, S., Rahman, M. A., ... & Abbas, F. I. (2022). Arduino based efficient energy storage systems using solar and wind power. *European Journal of Engineering and Technology Research, 7*(2), 134-139.
43. Al Rakib, M. A., Rahman, M. M., Anik, M. S. A., Masud, F. A. J., Rahman, M. A., Hossain, M. S., & Abbas, F. I. (2022). fire detection and water discharge activity for fire fighting robots using IoT. *European Journal of Engineering and Technology Research, 7*(2), 128-133.
44. Al Rakib, M. A., Rahman, M. M., Anik, M. S. A., Masud, F. A. J., Rahman, M. A., Islam, S., & Abbas, F. I. (2022). Arduino Uno based voice conversion system for dumb people. *European Journal of Engineering and Technology Research, 7*(2), 118-123.
45. Al Rakib, M. A., Uddin, S., Rahman, M. M., Chakraborty, S., & Abbas, F. I. (2021). Smart wheelchair with voice control for physically challenged people. *European Journal of Engineering and Technology Research, 6*(7), 97-102.
46. Al Rakib, M. A., Rahman, M. M., Samad, M., Islam, S., Rahman, M. A., & Abbas, F. I. (2021). Low-cost pulmonary ventilator for patient monitoring for Covid-19 disease. *European Journal of engineering and technology Research, 6*(6), 154-159.
47. Al Rakib, M. A., Rahman, M. M., Rana, M. S., Islam, M. S., & Abbas, F. I. (2021). GSM based home safety and security system. *European Journal of Engineering and Technology Research, 6*(6), 69-73.
48. Al Rakib, M. A., Rana, M. S., Rahman, M. M., & Abbas, F. I. (2021). Dry and wet waste segregation and management system. *European Journal of Engineering and Technology Research, 6*(5), 129-133.
49. Al Rakib, M. A., Mahamud, M. S., Zishan, M. S. R., & Abbas, F. I. (2021, July). An Arduino based smart hand gloves for load control and physician notification. In 2021 International Conference on Automation, Control and Mechatronics for Industry 4.0 (ACMI) (pp. 1-5). *IEEE.*
50. Ahmad, S., Mehedee, H. M., Bin, H. M. R., Hasan, R. R., Abbas, F. I., & Imam, M. H. (2021, January). Design of a compact simple structured dual-band patch antenna for wireless on-body medical and sports devices. In 2021 2nd International Conference on Robotics, Electrical and Signal Processing Techniques (ICREST) (pp. 577-581). *IEEE.*

Salah Uddin completed his graduation and postgraduate studies in physics and biomedical physics from the University of Dhaka in 2010 and 2015, respectively. Currently, he is a lecturer of physics in the faculty of EEE at Feni University. His research interests are oxide-based semiconductor materials, liquid binary alloys (mixing), IoT, and condensed matter physics.

Md. Miraj Hossain earned a master's degree in international studies from the Tokyo University of Foreign Studies, Japan. He previously received a bachelor's degree in international relations from the University of Dhaka, Bangladesh. He had done a professional course on SPSS statistics during his graduation. SPSS Statistics is a statistical software suite developed by the Dept. of Statistics & Informatics, University of Dhaka, for data management, advanced analytics, multivariate analysis, business intelligence, etc. After that, he is working in the broad realm of data science and simulation-based scientific investigation with his own research interests. However, he is very keen to make collaborative research into university-level research.